Brain Stimulation (2009) 2, 201 7

ELSEVIER

BRAIN
STIMULATION

www.brainstimjrnl.com

Gyri-precise head model of transcranial direct current stimulation: Improved spatial focality using a ring electrode versus conventional rectangular pad

Abhishek Datta, MS, Varun Bansal, BS, Julian Diaz, BS, Jinal Patel, MS, Davide Reato, MS, Marom Bikson, PhD

The City College of the City University of New York, New York, New York

The spatial resolution of conventional transcranial direct current stimulation (tDCS) is considered to be relatively diffuse owing to skull dispersion. However, we show that electric fields may be clustered at distinct gyri/sulci sites because of details in tissue architecture/conductivity, notably cerebrospinal fluid (CSF). We calculated the cortical electric field/current density magnitude induced during tDCS using a high spatial resolution (1 mm^3) magnetic resonance imaging (MRI) derived finite element human head model; cortical gyri/sulci were resolved. The spatial focality of conventional rectangular pad (7×5 cm^2) and the ring (4×1) electrode configurations were compared. The rectangular pad configuration resulted in diffuse (unfocal) modulation, with discrete clusters of electric field magnitude maxima. Peak induced electric field magnitude was not observed directly underneath the pads, but at an intermediate lobe. The 4×1 ring resulted in enhanced spatial focality, with peak induced electric field magnitude at the sulcus and adjacent gyri directly underneath the active electrode. Cortical structures may be focally targeted by using ring config urations. Anatomically accurate high resolution MRI based forward models may guide the "rational" clinical design and optimization of tDCS.

Keywords tDCS; focality; finite element modeling; MRI human head model; transcranial electrical stimulation

Conventional transcranial direct current stimulation (tDCS) involves weak direct currents (260 μA-2 mA) applied to the scalp via sponge-based rectangular pads (nominally 25-35 cm^2).[1-4] tDCS modulates cortical function and has been applied to facilitate learning, alter behavioral performance, and improve impaired brain function.[5-13]

A pivotal factor for tDCS efficacy and safety is the spatial extent of induced cortical electric field (EF)/current density. tDCS is considered to be poorly focused using rectangular-pad electrode configurations.[14-17] The spatial focality of induced cortical EF/current densities has been proposed to improve using reduced electrode sizes,[16-18] appropriate placement of electrodes,[15,17,19] and ring electrode configurations.[17] However, the precise role of complex tissue-compartment

This work was supported by National Institutes of Health (NIH) (nos. S06 GM008168 NS054783), Andy Grove Foundation, and PSC CUNY grants.

Correspondence: Marom Bikson, PhD, T 403 B Steinman Hall, Grove School of Engineering, The City College of the CUNY, 160 Convent Ave, New York, NY 10031.

E mail address: bikson@ccny.cuny.edu

Submitted December 13, 2008; revised March 12, 2009. Accepted for publication March 17, 2009.

1935 861X/09/$ see front matter © 2009 Elsevier Inc. All rights reserved.
doi:10.1016/j.brs.2009.03.005

morphology in influencing the flow of currents during tDCS has not been systematically addressed, including potential discrete cortical "hotspots" (clustering) of induced cortical EFs.[20-22]

During any transcranial current stimulation modality, the current that reaches the cortex is significantly altered from the applied scalp current because of intermediate tissue properties. A portion of the injected current is shunted across the scalp. The portion that crosses into the skull is then conducted by cerebrospinal fluid (CSF). Through the highly conductive CSF network, current can eventually cross into the brain. In the case of direct current (DC) stimulation, induced cortical currents/EFs have been shown to modulate the firing properties of neurons and "condition" neuronal excitability.[23-27] There is a general perception that the low conductivity of skull places a severe limit on the spatial focality of transcranial brain modulation.

One objective of this article was to compare the focality of "conventional" 7×5 cm^2 rectangular-pad stimulation with the 4×1 ring electrode configuration by using a high-resolution magnetic resonance imaging (MRI)-based finite element model (FEM) of the human head. Spherical-based[17,21] and MRI-derived[22,28] head models have previously been used to calculate tDCS electric fields. In this study, we incorporated gyri/sulci specificity by developing a model with 1 mm^3 resolution. Induced cortical EFs were used to predict relative spatial focality and the influence of tissue geometry/conductivity. We report that tDCS modulation maps are fundamentally influenced by detailed cortical architecture and re-evaluate perceived limitations on transcranial stimulation focality.

Methods

Volume conductor models were created with the same resolution (1 mm^3) as the MRI data used to derive them. Raw 3 T MRI scans were contrast enhanced and noise filtered. The head was segmented into compartments representing the brain tissue, CSF, skull, muscle, fatty tissue, eyes, blood vessels, and the scalp, respectively (Figure 1, A; Simpleware Ltd, Exeter, United Kingdom). The stimulation rectangular pads and disks were imported as CAD models (discussed later in text). The volumetric mesh was generated (minimum quality factor > 0.5) from the segmented data and eventually exported to COMSOL Multiphysics 3.4 (Comsol Inc, Massachusetts). The resulting mesh comprised $>$ 10,000,000 tetrahedral elements ($>$ 15,000,000 degrees of freedom).

The electrical properties of the tissues were assigned representative isotropic average values (in S/m): brain: 0.2; CSF: 1.65; skull: 0.01; and scalp: 0.465.[29-36] The muscle, fatty tissue, eyes, and blood vessel compartments were assigned the conductivity of scalp tissue.

We modeled two electrode configurations:

1. Rectangular pad (Figure 1, B): Two pads (7×5 cm^2) were placed at sites commonly used for tDCS of the primary motor cortex, with the "active" (anode) electrode over the left motor cortex and the "return" (cathode) electrode at the forehead above the contralateral orbita. Typically, the rectangular sponges are soaked in saline solution for conventional tDCS application and the abutting electrode is energized. The sponge was therefore assigned the conductivity of saline solution: 1.4 S/m.
2. 4×1 ring (Figure 1, C): To practically implement the concentric-ring configuration,[17] we approximated a ring using four "return" (cathode) disk electrodes arranged in a circular fashion around an "active" (anode) center electrode. The active electrode is placed over the motor cortex (coinciding with the center of the active pad used for rectangular-pad stimulation) and surrounded by four return electrodes (each at a disk center to disk center distance of 3 cm from the active electrode). The disk electrodes had a 4 mm radius. The 4×1 ring electrode system was implemented by passing current through disk electrodes into the scalp using a customized tDCS gel (CCNY-4) with conductivity: 0.3 S/m.

All electrodes had a thickness of approximately 1 mm and were modeled as conductors with the conductivity of copper: 5.8×10^7 S/m. The thickness of the CCNY-4 gel was approximately 2 mm, whereas the thickness of the sponge varied from 1-2.5 mm (thickness changed with scalp curvature to maintain continuous contact).

The Laplace equation $\nabla.(\sigma \nabla V) = 0$ (V: potential; σ: conductivity) was solved and the boundary conditions used were as follows: (1) inward current flow = J_n (normal current density) applied to the exposed surface of the anode electrode, (2) ground applied to the exposed surface of the cathode electrode(s), and (3) all other external surfaces treated as insulated. Current densities corresponding to 1 mA total current for the rectangular-pad configuration and 2 mA total current for the 4×1 ring configuration were respectively applied. These currents resulted in similar peak cortical-induced EF magnitude for each of the configurations. The finite element (FE) model was implemented using COMSOL. The linear system solver of conjugate gradients was used with a relative tolerance of 1×10^{-6}.

"Surface-magnitude" plots were generated by plotting the magnitude of EF on the surface of brain tissue. In addition, "cross-section magnitude" plots were generated by plotting the EF magnitude on coronal slices.[17] Because the conductivity of brain is uniform, these same plots also represent induced current density profiles (in which the actual current density values can be scaled using: $J = \sigma E$).

In this study, the induced brain EF magnitude was assumed to correlate with the degree of brain "modulation." The consideration of the EF (as opposed to the classical activating function) may be appropriate if: (1) tDCS-induced EFs are uniform at the scale of a neuron and (2) neuronal modulation may be directly correlated with uniform EF magnitude.[17,26,37-41] Our EF magnitude modulation maps do not consider any specific neuronal orientation (and target nonoriented structures).[17,42]

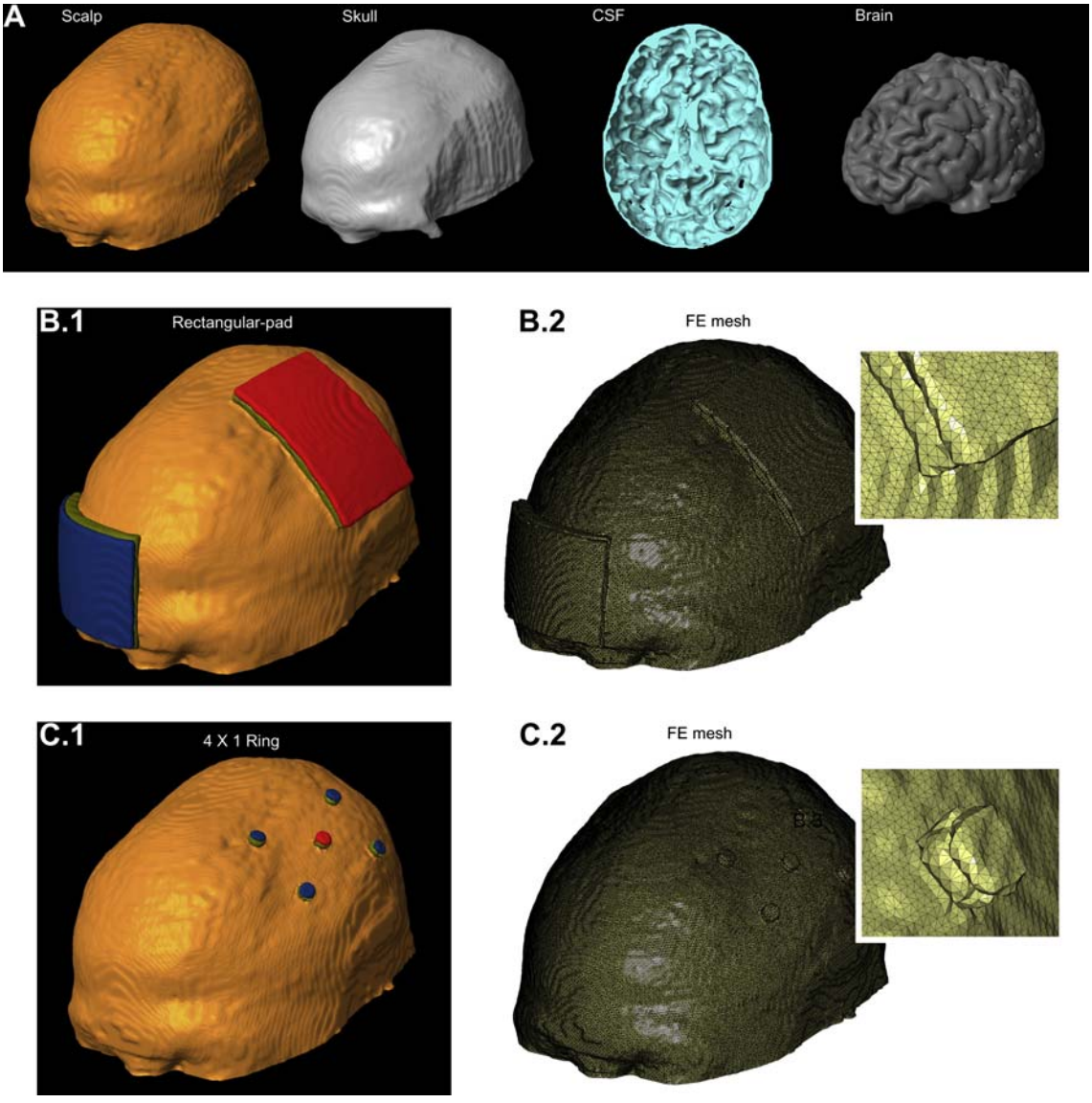

Figure 1 Finite element (FE) model of the conventional 7×5 cm^2 rectangular pad and 4×1 ring configurations. **A,** Segmented compartments in the following order: scalp, skull, cerebrospinal fluid (CSF), and brain. **B.1,** FE model of the conventional rectangular pad configuration and corresponding FE mesh (**B.2**). **C.1,** FE model of the 4×1 ring electrode configuration and corresponding FE mesh (**C.2**). The two insets show the zoomed mesh images, highlighting finer detail. Red: anode electrode; Blue: cathode electrode(s); Olive green: sponge/gel.

Results

For the 7×5 cm^2 rectangular pad and the 4×1 ring configuration models (Figure 1, B and C), we calculated the induced EF/current density magnitude in the brain. The surface-magnitude/cross-section magnitude EF plots for each of the configurations allow a direct comparison of relative cortical surface and depth focality (Figure 2).

Rectangular-pad stimulation with 7×5 cm^2 pads results in widespread diffuse (unfocal) modulation over the entire cortical surface because of the large size and separation of pads (Figure 2, A.2). Total current of 1 mA injected through the pads results in 0.67 V/m peak cortical EF magnitude (encompassed in dashed region of Figure 2, A.2; expanded in Figure 2, A.4) in the walls of a frontal lobe gyrus. The peak cortical EF magnitude of 0.67 V/m corresponds to 0.13 A/m^2 peak cortical current density magnitude. The local EF magnitude peak directly underneath the pads was 0.45 V/m. The minimum cortical-induced EF magnitude in the entire frontal area of the brain was approximately 0.16 V/m (see coronal slice, Figure 2, A.6) and approximately 0.06 V/m in the occipital area.

The presence of distinct clusters of EF magnitude maxima (Figure 2, A.2) was influenced by regions of reduced skull thickness, which may provide preferential current pathways of current crossing into the CSF (Supplementary Figure), as well as channels of high-conductivity CSF bounded by brain and skull. For example, a particular

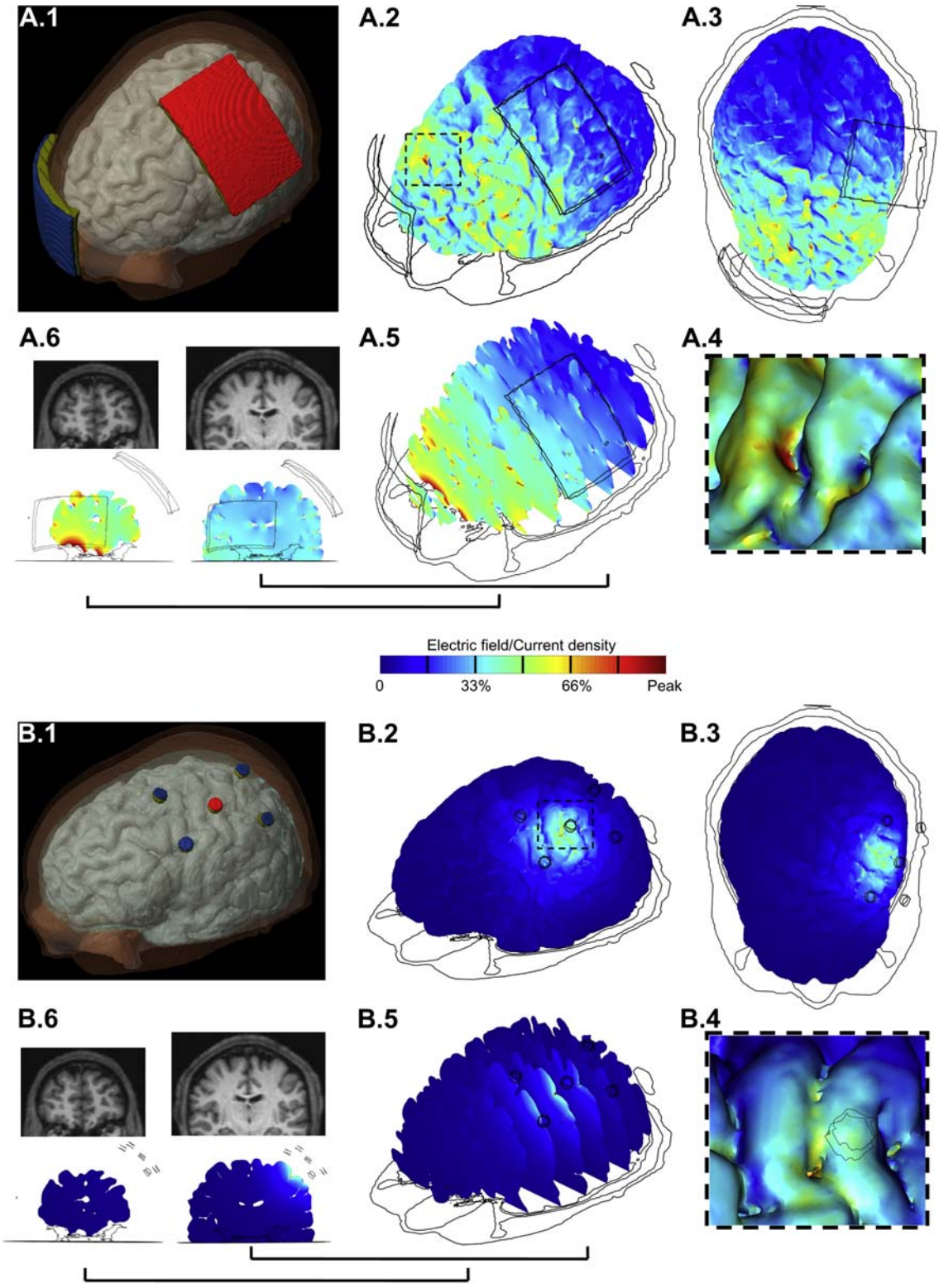

Figure 2 Brain modulation during transcranial direct current stimulation (tDCS) using conventional rectangular pad configuration (**A.1**) and the 4 × 1 ring electrode configuration (**B.1**). Red: anode electrode; Blue: cathode electrode(s); Olive green: sponge/gel. For each config uration, we calculated the induced cortical electric field (EF) **magnitude**. **A.2** and **B.2,** S*urface magnitude* plots of EF along the brain surface, same view as **A.1** and **B.1**. The dashed region is expanded in inset (**A.4**). **A.3** and **B.3,** *Top view* of the brain showing the induced s*urface magnitude* EF. The insets (**A.4**) and (**B.4**) show the zoomed *surface magnitude* EF plots. These images are obtained with "lighting" on [COMSOL Multiphysics] to highlight gyri/sulci modulation. **A.5** and **B.5,** *Cross section magnitude* EF plotted on a series of successive cortical slices, same view as **A.1** and **B.1**. The *cross section magnitude* EF plots for two slices and their corresponding magnetic resonance

gyrus may have high-induced EF magnitude caused by wide pockets of CSF on either side acting as a current "sink"[36] as well as reduced CSF thickness over that gyri crown acting as a "funnel."

The 4×1 ring configuration leads to a significant increase in spatial focality (Figure 2, B.2). Peak EF magnitude is observed in the gyri and the intermediate sulcus directly underneath the active stimulation electrode (coronal slice, Figure 2, B.6). The region of modulation is generally constrained between the active electrode and the four return electrodes with a 0.44 V/m EF magnitude peak (encompassed in dashed region of Figure 2, B.2; expanded in Figure 2, B.4). Thus, by using the 4×1 ring configuration, 2 mA resulted in a comparable peak EF magnitude in the motor cortex as 1 mA rectangular-pad (7×5 cm^2) stimulation. However, for the 4×1 ring configuration, there was no cortical modulation (< 0.01 V/m) in the frontal regions, on the contralateral (right) motor regions of the brain, or on the occipital lobe of the brain. The overall spatial profile of brain modulation was strongly influenced by tissue inhomogeneity, notably because of CSF (Supplementary Figure).

Discussion

The translation of stimulation models to clinical applications requires reproducing application-appropriate anatomic features.[43-50] The incorporation of gyri/sulci specificity in our three-dimensional (3D) human head model can guide rational tDCS design and optimization.[42,51]

The overall current flow caused by any transcranial electric stimulation is complex and is influenced by a convergence of factors including: (1) electrode size/geometry and separation-distance, with related scalp shunting[17]; (2) skull thickness, presence of sutures, and eye cavities; (3) channels of high conductivity CSF enclosing/and perfusing the underlying cortex; (4) convoluted brain surface morphology; and (5) differences in tissue conductivities at boundaries between tissue compartments.

tDCS using conventional "large" rectangular pads resulted in diffuse (unfocal) cortical modulation. Moreover, the complex geometry of the brain and regional differences in conductance cause local nonuniformities of current density through the CSF (eg, "sinks" and "funnels") that are reflected in clustering of brain EF magnitude at distinct sites. Indeed, some imaging and physiological studies suggest diffuse brain modulation and clustering of regional cerebral blood flow/EF, independent of anatomic connections.[20,52] Separate imaging, TMS mapping studies and, clinical studies indicate some level of functional spatial selectivity,[1,5,7-9] which may be explained by FE models with more specific modulation maps,[17] including nonlinearities and thresholding. Whereas, our EF magnitude modulation maps assume no particular neuronal geometry or waveform dependent biophysical transduction mechanisms, direction-specific modulation maps incorporating cellular orientation (radial versus tangential)[17] and EF derivative (classical activating function)[53,54] have been applied elsewhere.[43,44,47] In cases of pulsed or AC stimulation waveforms, the appropriate modulation map (parameter/function that determines degree of brain "modulation") may differ.[20,55,56]

Any FE human head model is limited by the accuracy of tissue dimensions and conductivity values incorporated (inhomogeneity and anisotropy). The current study investigated the distribution of tDCS- induced currents in brain using a highly detailed anatomic model. The high MRI scan resolution (1 mm^3) allows accurate segmentation of individual tissue compartments. Consequently, the precise 3D model rendered, captures anatomic detail such as cortical folding (Figure 2, A.4). Finally, the precise FE mesh generated (> 10 million elements), allows accurate computation of induced fields. The importance of incorporating gyri/sulci specificity is highlighted by the observance of clustering of brain modulation during conventional tDCS (Supplementary Figure). Our results also suggest that individual variability would affect the magnitude and spatial extent of cortical electric fields. For example, young children have vascularized fontanels, among adults there are differences in the degree/timing of suture closing[36] and elderly subjects have larger fractional CSF volumes.[57]

Our computational results suggest that the focality of clinical tDCS application can be significantly enhanced by the 4×1 ring configuration. In addition, because the peak-induced cortical EF magnitude is similar to the rectangular-pad stimulation, the 4×1 ring results in more targeted brain modulation (hence, potentially a safer electrode configuration). The peak cortical current density of 0.09 A/m^2 induced underneath the pads by rectangular pad (1 mA) and 4×1 ring (2 mA) configurations are more than two orders of magnitude away from the threshold for histopathologically observed tDCS brain damage in a rat model.[58] We emphasize that using the 4×1 ring configuration, the more *surface* current needed does not lead to more peak-induced cortical EF magnitude, but reflects shunting across the scalp (without crossing into the brain).[59]

For skin safety, the increased scalp current associated with 4×1 ring can be offset by increasing the separation distance between stimulation electrodes, but at the cost of stimulation

imaging (MRI) scans are shown in **A.6** and **B.6**. One slice is chosen directly from underneath the rectangular pad/active electrode of 4×1 ring configuration and another from the prefrontal area of the brain. The same slices are shown for each of the configurations. All plots are normalized between zero and the peak positive cortical EF magnitude: conventional rectangular pad peak = 0.67 V/m (or 0.13 A/m^2 current density peak); 4×1 ring peak = 0.44 V/m. (Note that for the rectangular pad, the EF magnitude peak is observed between the pads and not underneath).

focality.[17] Importantly, when conventional sponge electrodes are used, the current density at the scalp is, in fact, concentrated at the sponge edges and thus exceeds the average current density (injected current/electrode surface area).[21,22] Moreover, electrode materials and design are as pivotal to comfort as is average current density;[60-62] by using appropriate hardware (electrode adapters, stimulation gels), 39.8 A/m^2 current density may be applied without pain.[63] Because of the previously discussed issues, pain perception for skin should be addressed in a clinical study.[64] Thus, electrode designs that mitigate skin irritation should be developed along with electrode configurations that enhance spatial focality.

The quasistatic field approximation implies conservation and linearity of EF solution. Thus, our EF magnitude "spatial profile" results can be extrapolated to other transcranial current stimulation modalities (eg, suprathreshold transcranial electrical stimulation, electroconvulsive therapy, transcranial alternating current stimulation, transcranial random noise stimulation, and cranial electrotherapy stimulation),[20,55,56,65,66] where the 4×1 ring configuration may be used to focally target cortical structures.

The "transparency" of the skull to magnetic stimulation has led to the development of specialized coils for focused transcranial magnetic stimulation.[50,67-70] There is a general perception that the low conductivity of skull places a severe limit on spatial focality of transcranial electrical stimulation, including tDCS. However, the results of this modeling study support the further development of transcranial current stimulation technology for focal stimulation.

Acknowledgements

We acknowledge Ross Cotton of Simpleware Ltd and Konrad Juethner of Comsol Inc. We also thank Pejman Sehatpour at Nathan Kline Institute; Thomas Radman, Fortunato Battaglia, and Lucas Parra of the City College of New York.

References

1. Nitsche MA, Paulus W. Excitability changes induced in the human motor cortex by weak transcranial direct current stimulation. J Physiol 2000;527:633 639.
2. Marshall L, Molle M, Siebner HR, Born J. Bifrontal transcranial direct current stimulation slows reaction time in a working memory task. BMC Neurosci 2005;6:23.
3. Iyer MB, Mattu U, Graffman J, et al. Safety and cognitive effect of frontal DC brain polarization in healthy individuals. Neurology 2005;64:872 875.
4. Hummel F, Celnik P, Giraux P, et al. Effects of non invasive cortical stimulation on skilled motor function in chronic stroke. Brain 2005; 128:490 499.
5. Nitsche MA, Schauenburg A, Lang N, et al. Facilitation of implicit motor learning by weak transcranial direct current stimulation of the primary motor cortex in the human. J Cogn Neurosci 2003;15:619 626.
6. Uy J, Ridding MC. Increased cortical excitability induced by transcra nial DC and peripheral nerve stimulation. J Meurosci Methods 2003; 127:193 197.
7. Kincses TZ, Antal A, Nitsche MA, Bartfai O, Paulus W. Facilitation of probabilistic classification learning by transcranial direct current stim ulation of the prefrontal cortex in the human. Neuropsychologia 2004; 42:113 117.
8. Antal A, Kincses TZ, Nitsche MA, Bartfai O, Paulus W. Excitability changes induced in the human primary visual cortex by transcranial direct current stimulation: direct electrophysiological evidence. Invest Ophthalmol Vis Sci 2004;45(2):702 707.
9. Boggio PS, Bermpohl F, Vergara AO, et al. Go no go task perfor mance improvement after anodal transcranial DC stimulation of the left dorsolateral prefrontal cortex in major depression. J Affect Disord 2006;101:91 98.
10. Liebetanz D, Klinker F, Hering D, et al. Anticonvulsant effects of transcranial direct current stimulation (tDCS) in the rat cortical ramp model of focal epilepsy. Epilepsia 2006;47:1216 1224.
11. Boggio PS, Ferrucci R, Rigonatti SP, et al. Effects of transcranial direct current stimulation on working memory in patients with parkin son's disease. J Neurol Sci 2006;249:31 38.
12. Fregni F, Boggio PS, Lima MC, et al. A sham controlled, phase II trial of transcranial direct current stimulation for the treatment of central pain in traumatic spinal cord injury. Pain 2006;122:197 209.
13. Boggio PS, Khoury LP, Martins DC, Martins OE, de Macedo EC, Fregni F. Temporal cortex DC stimulation enhances performance on a visual recognition memory task in Alzheimer's disease. J Neurol Neurosurg Psychiatry 2009;80:444 447.
14. Rossini PM, Marciani MG, Caamia M, Roma V, Zarola F. Nervous propagation along 'central' motor pathways in intact man: character istics of motor responses to 'bifocal' and 'unifocal' spine and scalp non invasive stimulation. Electroencephalogr Clin Neurophysiol 1985;61:272 286.
15. Nathan SS, Sinha SR, Gordon B, Lesser RP, Thakor NV. Determina tion of current density distributions generated by electrical stimulation of the human cerebral cortex. Electroencephalogr Clin Neurophysiol 1993;86:183 192.
16. Nitsche MA, Doemkes S, Karakose T, et al. Shaping the effects of transcranial direct current stimulation of the human motor cortex. J Neurophysiol 2007;97:3109 3117.
17. Datta A, Elwassif M, Battaglia F, Bikson M. Transcranial current stim ulation focality using disc and ring electrode configurations: FEM analysis. J Neural Eng 2008;5:163 174.
18. Kwon YH, Ko MH, Ahn SH, et al. Primary motor cortex activation by transcranial direct current stimulation in the human brain. Neurosci Lett 2008;435:56 59.
19. Borckardt JJ, Linder KJ, Ricci R, et al. Focal electrically administered therapy: device parameter effects on stimulus perception in humans [pub lished online ahead of print December 12, 2008]. J ECT 2009;25:91 98.
20. Kanai R, Chaieb L, Antal A, Walsh V, Paulus W. Frequency depend ent electrical stimulation of the visual cortex. Curr Biol 2008;18(23): 1839 1843.
21. Miranda PC, Lomarev M, Hallett M. Modeling the current distribution during transcranial direct current stimulation. Clin Neurophysiol 2006; 117:1623 1629.
22. Wagner T, Fregni F, Fecteau S, Grodzinsky A, Zahn M, Pascual Leone A. Transcranial direct current stimulation: a computer based human model study. Neuroimage 2007;35:1113 1124.
23. Purpura DP, McMurty JG. Intracellular activities and evoked potential changes during polarization of motor cortex. J Neurophysiol 1965;28: 166 185.
24. Bindman LJ, Lippold OCJ, Redfearn JWT. The action of brief polarizing currents on the cerebral cortex of the rat (1) during current flow and (2) in the production of long lasting after effects. J Physiol 1964;172:369 382.
25. Gartside IB. Mechanisms of sustained increases of firing rate of neurons in the rat cerebral cortex after polarization: role of protein synthesis. Nature 1968;220:383 384.
26. Bikson M, Inoue M, Akiyama H, et al. Effects of uniform extracellular DC electric fields on excitability in rat hippocampal slices in vitro. J Physiol 2004;557:175 190.

27. Radman T, Su Y, An JH, Parra LC, Bikson M. Spike timing amplifies the effect of electric fields on neurons: implications for endogenous field effects. J Neurosci 2007;27:3030 3036.
28. Oostendorp TF, Hengeveld YA, Wolters CH, Stinstra J, van Elswijk G, Stegeman DF. Modeling transcranial DC stimulation. Conf Proc IEEE Eng Med Biol Soc 2008;2008:4226 4229.
29. Geddes LA, Baker LE. The specific resistance of biological materi al—a compendium of data for the biomedical engineer and physiolo gist. Med Biol Eng 1967;5:271 293.
30. Akhtari M, Bryant HC, Mamelak AN, et al. Conductivities of a three layer live human skull. Brain Topogr 2002;14(3):151 167.
31. Ranck JB. Specific impedance of rabbit cerebral cortex. Exp Neurol 1963;7:144 152.
32. Baumann SB, Wozny DR, Kelly SK, Meno FM. The electrical conductivity of human cerebrospinal fluid at body temperature. IEEE Trans Biomed Eng 1997;44(3):220 223.
33. Gabriel C, Gabriel S, Corthout E. The dielectric properties of biolog ical tissues: I, literature survey. Phys Med Biol 1996;41(11): 2231 2249.
34. Hauesien J, Ramon C, Eiselt M, Brauer H, Nowak H. Influence of tissue resistivities on neuromagnetic fields and electric potentials studied with a finite element model of the head. IEEE Trans Biomed Eng 1997;44(8):727 735.
35. Nadeem M, Thorlin T, Gandhi OP, Persson M. Computation of electric and magnetic stimulation in human head using the 3 D impedance method. IEEE Trans Biomed Eng 2003;50:900 907.
36. Holdefer RN, Sadleir R, Russell MJ. Predicted current densities in the brain using transcranial electrical stimulation. Clin Neurophysiol 2006;117:1388 1397.
37. Tranchina D, Nicholson C. A model for the polarization of neurons by extrinsically applied electric fields. J Biophys 1986;50:1139 1156.
38. Nagarajan SS, Durand DM, Warman EN. Effects of induced electric fields on finite neuronal structures: a simulation study. IEEE Trans Biomed Eng 1993;40:1175 1188.
39. Amassian VE, Eberle L, Maccabee PJ, Cracco RQ. Modelling magnetic coil excitation of human cerebral cortex with a peripheral nerve immersed in a brain shaped volume conductor: the significance of fibre bending in excitation. Electroencephalogr Clin Neurophysiol 1992;85:291 301.
40. Roth BJ. Mechanisms for electrical stimulation of excitable tissue. Crit Rev Biomed Eng 1994;22:253 305.
41. Chan CY, Nicholson C. Modulation by applied electric fields of purkinje and stellate cell activity in the isolated turtle cerebellum. J Physiol 1986;371:89 114.
42. Bikson M, Bulow P, Stiller JW, et al. Transcranial direct current stimulation for major depression: a general system for quantifying transcranial electrotherapy dosage. Curr Treat Options Neurol 2008; 10(5):377 385.
43. Johnson MD, McIntyre CC. Quantifying the neural elements activated and inhibited by global pallidus deep brain stimulation 2008;100(5): 2549 2563.
44. Wongsarnpigoon A, Grill WM. Computational modeling of epidural cortical stimulation. J Neural Eng 2008;5(4):443 454.
45. Im CH, Jung HH, Choi JD, Lee SY, Jung KY. Determination of optimal electrode positions for transcranial direct current stimulation (tDCS). Phys Med Biol 2008;53:219 225.
46. Manola L, Holsheimer J, Veltink P, Buitenweg JR. Anodal vs cathodal stimulation of motor cortex: a modeling study. Clin Neurophysiol 2007;118:464 474.
47. Butson CR, Cooper SE, Henderson JM, McIntyre CC. Patient specific analysis of the volume of tissue activated during deep brain stimula tion. Neuroimage 2007;34(2):661 670.
48. Holsheimer J. Computer modelling of spinal cord stimulation and its contribution to therapeutic efficacy. Spinal Cord 1998;36(8):531 540.
49. De Lucia M, Parker GJM, Embleton K, Newton JM, Walsh V. Diffu sion tensor MRI based estimation of the influence of brain tissue anisotropy on the effects of transcranial magnetic stimulation. Neuro image 2007;36:1159 1170.
50. Deng ZD, Peterchev AV, Lisanby SH. Coil design considerations for deep brain transcranial magnetic stimulation (dTMS). Conf Proc IEEE Eng Med Biol Soc 2008;2008:5675 5679.
51. Bikson M, Radman T, Datta A. Rational modulation of neuronal pro cessing with applied electric fields. Conf Proc IEEE Eng Med Biol Soc 2006;1:1616 1619.
52. Lang N, Siebner HR, Ward NS, et al. How does transcranial DC stim ulation of the primary motor cortex alter regional neuronal activity in the human brain? Eur J Neurosci 2005;22:495 504.
53. Rattay F. Analysis of models for external stimulation of axons. IEEE Trans Biomed Eng 1986;33:974 977.
54. Plonsey R, Barr RC. Electric field stimulation of excitable tissue. IEEE Trans Biomed Eng 1995;42:329 336.
55. Terney D, Chaieb L, Moliadze V, Antal A, Paulus W. Increasing human brain excitability by transcranial high frequency random noise stimulation. J Neurosci 2008;28(53):14147 14155.
56. Lisanby SH. Electroconvulsive therapy for depression. N Eng J Med 2007;357:1939 1945.
57. Murphy DG, DeCarli C, Schapiro MB, Rapoport SI, Horwitz B. Age related differences in volumes of subcortical nuclei, brain matter, and cerebrospinal fluid in healthy men as measured with magnetic resonance imaging. Arch Neurol 1992;49(8):839 845.
58. Liebetanz D, Koch R, Mayenfels S, et al. Safety limits of cathodal transcranial direct current stimulation in rats. Clin Neurophysiol 2009;120:1161 1167.
59. Bikson M, Datta A, Elwassif M. Establishing safety limits for transcra nial direct current stimulation. Clin Neurophysiol 2009;120:1033 1034.
60. Dundas JE, Thickbroom GW, Mastaglia FL. Perception of comfort during transcranial direct current stimulation: effect of NaCl solution concentration applied to sponge electrodes. Clin Neurophysiol 2007; 118:1166 1170.
61. Palm U, Keeser D, Schiller C, et al. Skin lesions after treatment with transcranial direct current stimulation (tDCS). Brain Stimulation 2008; 1:386 387.
62. Merrill DR, Bikson M, Jefferys JG. Electrical stimulation of excitable tissue: design of efficacious and safe protocols. J Neurosci Methods 2005;141:171 198.
63. Prausnitz MR. The effects of electric current applied to skin: a review for transdermal drug delivery. Adv Drug Deliv Rev 1996;18: 395 425.
64. Arana AB, Borckardt JJ, Ricci R, et al. Focal electrical stimulation as a sham control for repetitive transcranial magnetic stimulation: does it truly mimic the cutaneous sensation and pain of active prefrontal repetitive transcranial magnetic stimulation? Brain Stimulation 2008; 1:44 51.
65. Calancie B, Harris W, Broton JG, Alexeeva N, Green BA. 'Threshol d level' multipulse transcranial electrical stimulation of motor cortex for intraoperative monitoring of spinal motor tracts: description of method and comparison to somatosensory evoked potential moni toring. J Neurosurg 1998;88:457 470.
66. Schroeder MJ, Barr RE. Quantitative analysis of the electroencephalo gram during cranial electrotherapy stimulation. Clin Neurophysiol 2001;112:2075 2083.
67. Cohen LG, Roth BJ, Nilsson J, et al. Effects of coil design on delivery of focal magnetic stimulation: technical considerations. Electroence phalogr Clin Neurophysiol 1990;75:350 357.
68. Ren C, Tarjan PP, Popovic DB. A novel electric design for electromag netic stimulation—the slinky coil. IEEE Trans Biomed Eng 1995;42: 918 925.
69. Ruohonen J, Ilmoniemi RJ. Focusing and targeting brain stimulation using multiple coils. Med Biol Eng Comput 1998;36:297 301.
70. Roth Y, Zangen A, Hallett M. A coil design for transcranial magnetic stimulation of deep brain regions. J Clin Neurophysiol 2002;19: 361 370.

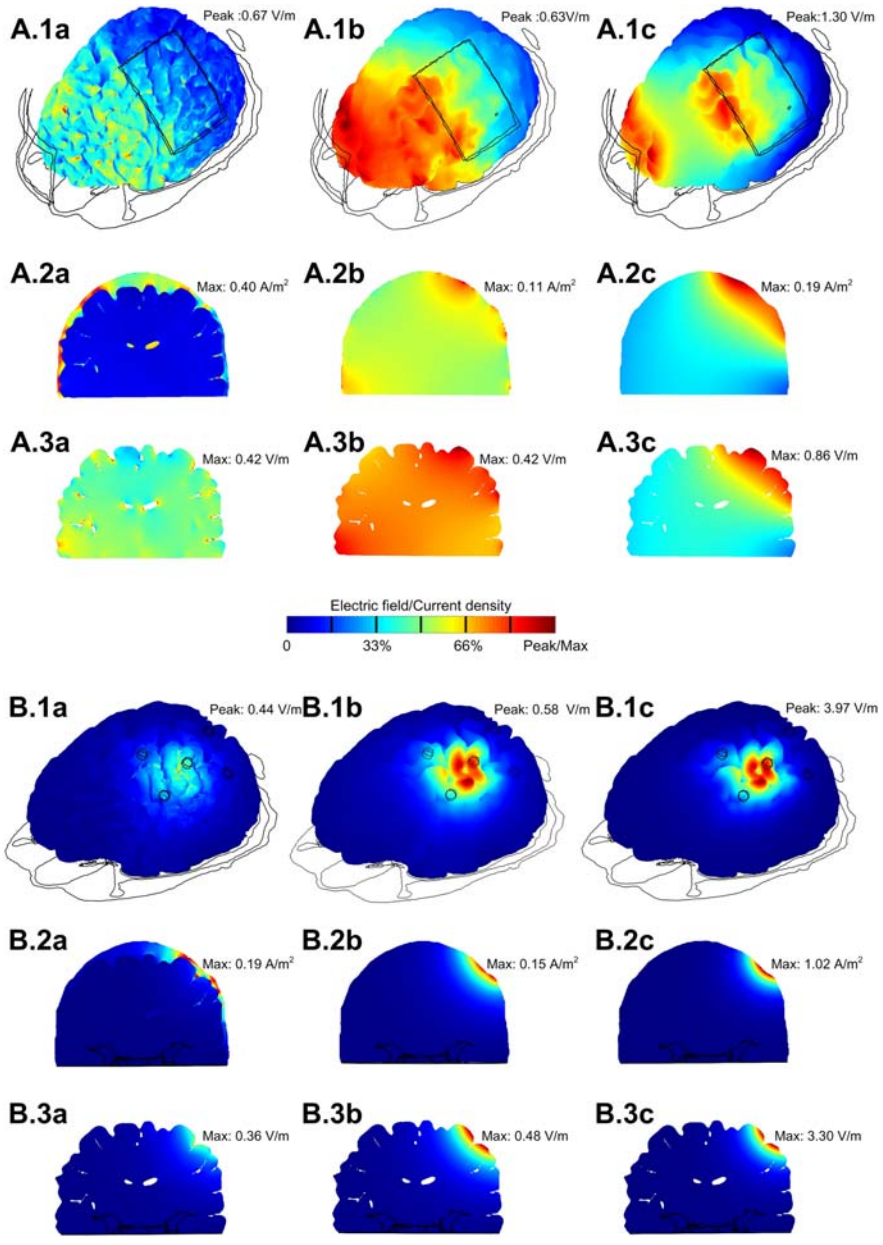

Supplementary Figure Influence of tissue properties on the spatial profiles of electric field (EF)/current density magnitudes induced by stimulation with rectangular pad (**A**) and 4 × 1 ring (**B**) electrode configurations. First column: simulation results with *inhomogeneous* electrical conductivities. Second column: simulation results using the same head model but with $\sigma_{CSF} = \sigma_{brain} = 0.2$ S/m. Third column: simulation results with *homogeneous* tissue conductivity ($\sigma = 0.2$ S/m). Rows **A.1** and **B.1**: Cortical *surface-magnitude* electric fields. Rows **A.2** and **B.2**: Induced *current density* magnitude in both CSF and brain on a single cross-sectional slice (same slice as in Figure 2). Rows **A.3** and **B.3**: Cortical *Cross-section magnitude* EFs. For the rectangular-pad stimulation, sites of high current densities in CSF generally correspond with regions of high-induced cortical EF magnitudes that are reflected as distinct clusters of modulation (**A.2a** and **A.3a**). Note that **A.1a** and **B.1a** are same as Figure 2, **A.2** and **B.2**. When the brain and CSF compartments have same conductivity, the region of peak induced EFs roughly encompasses the entire cortical surface between the pads (**A.1b**). In addition, distinct clustering of EFs is not observed owing to similar electrical properties and absence of convoluted cortical morphology (**A.2b** and **A.3b**). The cortical surface comprising the peak induced EF magnitudes demonstrates regions of reduced skull thickness (**A.1b**). Two distinct peaks of modulation beneath the two corresponding rectangular pads are observed when homogeneous conductivities are considered (**A.1c**). For the 4 × 1 ring configuration, the region of peak cortical EF magnitude corresponds to sites of high-induced current densities in CSF (**B.3a** and **B.2a**) similar to rectangular-pad simulation. For the homogeneous case and when the brain and CSF compartments have same conductivity, region of peak-induced EFs roughly encompasses the cortical surface between the active and return electrodes (**B.1b** and **B.1c**). Note that for the cross-sectional plots (Rows: **A.2**, **A.3**, **B.2**, **B.3**) the maximum has been scaled for clarity as indicated.